Bioorg. Med. Chem. Lett. 66 (2022) 128725

Contents lists available at ScienceDirect

Bioorganic & Medicinal Chemistry Letters

journal homepage: www.elsevier.com/locate/bmcl

Stapled peptides as scaffolds for developing radiotracers for intracellular targets: Preliminary evaluation of a radioiodinated MDM2-binding stapled peptide in the SJSA-1 osteosarcoma model

Zhengyuan Zhou, Michael R. Zalutsky, Satish K. Chitneni *

Department of Radiology, Duke University Medical Center, Durham, NC 27710, United States

ARTICLE INFO

Keywords:
Stapled peptide
MDM2
VIP116
SJSA-1
Radioiodine

ABSTRACT

Stapled peptides are promising scaffolds for inhibiting protein–protein interactions in cells, including between the intracellular oncoprotein MDM2 and p53. Herein, we have investigated the potential utility of a stapled peptide, VIP116, for developing radiolabeled agents targeting MDM2. VIP116 was radioiodinated using the prosthetic agent *N*-succinimidyl-3-[*I]iodobenzoate ([*I]SIB). The resulting labeled peptide [*I]SIB-VIP116 exhibited high uptake (165.3 ± 27.7%/mg protein) and specificity in SJSA-1 tumor cells. Tissue distribution studies of [*I]SIB-VIP116 revealed a peak tumor uptake of 2.19 ± 0.56 percent injected dose per gram (%ID/g) in SJSA-1 xenografts at 2 h post-injection, which was stable until 6 h. [*I]SIB-VIP116 exhibited high activity (8.33 ± 1.18%ID/g) in the blood pool but had high tumor-to-muscle ratios (12.0 ± 5.7), at 30 min. Metabolic stability studies in mice indicated that about 80% of the activity in plasma was intact [*I]SIB-VIP116 at 4 h. Our results confirm the cell permeability and specific binding of [*I]SIB-VIP116 to MDM2 and the suitability of the VIP116 scaffold for radiolabeled probe development.

Peptide radiopharmaceuticals have made significant advances in the past few years, exemplified by FDA approval of [^{68}Ga]Ga-DOTA-TATE and [^{177}Lu]Lu-DOTA-TATE for imaging and targeted radiotherapy of somatostatin receptor-overexpressing neuroendocrine tumors, respectively.[1,2] Additionally, other radiolabeled peptides are currently in clinical trials for targeting receptors and antigens that are overexpressed in cancers including integrins, gastrin-releasing peptide receptors, and PD-L1.[3–5] Peptides offer significant flexibility for designing and developing radiopharmaceuticals with high target affinity and selectivity, compatibility with appropriate radionuclides for diagnostic and therapeutic applications, and for optimizing target-to-background ratios in vivo. However, linear peptides have several limitations that prevent them from being efficient molecular scaffolds for radiopharmaceutical development, especially for intracellular targets, because of their limited cell permeability and susceptibility to proteolytic degradation in vivo.[6] Consequently, the majority of the radiolabeled peptides that have been successfully translated to clinical trial have been cyclic peptides and/or for targeting cell surface receptors or antigens.[5,7,8]

Stapled peptides are a relatively new class of peptides wherein two α-methyl olefin containing artificial amino acids are introduced on the main peptide backbone and are covalently crosslinked via a ring-closing metathesis to induce a peptide α-helical structure.[9] Peptide stapling has been shown to address some of the limitations mentioned above for linear peptides. Peptide stapling confers higher α-helicity resulting in increased target binding affinity, improved cell permeability, and stability towards proteolytic degradation.[10–12] To date, several stapled peptides have been developed for inhibiting a variety of protein–protein interactions (PPIs) inside the cells.[9] Of those, stapled peptides that inhibit the interaction of murine double minute 2 (MDM2) with p53 are among the most advanced, illustrated by ALRN-6924, the first stapled peptide to enter clinical trial.[13,14] MDM2-binding stapled peptides are designed based on the native p53 interaction with MDM2 and bind to the highly conserved p53-binding pocket on the *N*-terminus of the MDM2 protein by mimicking hydrophobic residues Phe19, Trp23 and Leu26 on the p53 protein.[10] p53 is of high interest because it plays a crucial role in the cellular response to stress signals such as DNA damage and in preventing cancer formation.[15] In unstressed cells, p53 levels are kept low by MDM2, which induces rapid degradation of the p53 protein via its E3 ubiquitin ligase activity.[16,17] However, MDM2 is overexpressed in several cancers, thereby leading to the continued suppression of the p53 pathway and promoting tumor growth.[18,19] Thus, MDM2 inhibition with small molecules or stapled peptides has the potential to

* Corresponding author.
E-mail address: satish.chitneni@duke.edu (S.K. Chitneni).

https://doi.org/10.1016/j.bmcl.2022.128725
Received 9 March 2022; Received in revised form 4 April 2022; Accepted 6 April 2022
Available online 15 April 2022

activate the p53 pathway and induce apoptosis or cell cycle arrest in wild-type p53 cancers.[10,11,20,21]

VIP116, first reported by Thean et al., is a rationally designed stapled peptide with a high binding affinity towards MDM2 (K_d = 15.1 ± 1.7 nM) and has been shown to induce p53 levels in tumor cells in vitro and in a B16F10 melanoma allograft tumor model in vivo.[22–24] Additionally, PM2, a predecessor peptide to VIP116, has been shown to potentiate the therapeutic effects of radiation treatment delivered via external beam or targeted radiotherapy using a ^{177}Lu-labeled antibody binding CD44v6 in the HCT116 colorectal cancer model.[25,26] In both cases, MDM2 inhibition with the stapled peptide PM2 improved the therapeutic efficacy of the corresponding radiation treatment by inducing p53 levels in HCT116 tumor spheroids or tumor xenografts in vivo.[25,26]

While several cyclic peptides have been successfully developed and translated to clinical evaluation,[5,7,27] stapled peptides have been largely unexplored for radiopharmaceutical development, specifically for intracellular targets such as MDM2. Herein, we investigated the in vitro and in vivo characteristics of the above-described MDM2-binding stapled peptide VIP116, radioiodinated using the prosthetic agent *N*-succinimidyl-3-[*I]iodobenzoate ([*I]SIB), in the SJSA-1 osteosarcoma model. We show that the radioiodinated peptide [*I]SIB-VIP116 permeates the cell membrane and binds to MDM2 with high specificity in tumor cells. Furthermore, the stapled peptide has a favorable normal tissue distribution profile and metabolic stability in vivo after intravenous administration in mice.

Radioiodination of VIP116 was achieved by conjugating the dehalogenation-resistant radioiodination prosthetic agent *N*-succinimidyl-3-[*I]iodobenzoate ([*I]SIB) to a lysine residue connected via an aminohexanoic spacer at the *N*-terminus of the peptide (Scheme 1). In this study, we employed ^{125}I for radioiodination of [*I]SIB in most experiments; however, [*I]SIB could be labeled with ^{123}I or ^{124}I for SPECT and PET imaging, respectively. First, nonradioactive [^{127}I]SIB-VIP116 was synthesized via the standard acylation reaction by incubating VIP116 with *N*-succinimidyl ester-activated 3-iodobenzoate ([^{127}I]SIB) in DMF in the presence of diisopropylethylamine at room temperature for 1 h. After the reaction, the [^{127}I]SIB-conjugated VIP116 was purified using a reversed-phase HPLC (RP-HPLC) system to obtain the nonradioactive peptide conjugate [^{127}I]SIB-VIP116 in 65% yield. The identity of the conjugated peptide was confirmed by high-resolution mass spectrometry, which revealed a molecular mass of 1162.5303 Da (calculated, 1162.5306 Da; $[M+2H]^{2+}$), consistent with the chemical structure of [^{127}I]SIB-VIP116 (Fig. S1).

The inhibitory potency of the nonradioactive peptide conjugate towards MDM2 was determined by competitive inhibition assays using a carboxyfluorescein (5-FAM) labeled p53-based peptide, 5-FAM-PMDM6 (sequence: 5-FAM-βAla-βAla-**Phe**-Met-Aib-pTyr-(6-Cl-DL-**Trp**)-Glu-Ac3c-**Leu**-Asn-NH_2, AnnaSpec, Inc.), and recombinant human MDM2 protein (E3-204, R&D Systems) in a fluorescence polarization-based assay as described previously.[28] In brief, increasing concentrations of [^{127}I]SIB-VIP116 or unmodified VIP116 were added to a pre-incubated 5-FAM-PMDM6:MDM2 complex and measured for fluorescence polarization at 3 h post-incubation. From these data, the peptide concentration at which half of the bound 5-FAM-PMDM6 was displaced from the MDM2 protein was determined (IC_{50}) by nonlinear fitting of the data using equation log(inhibitor) vs. response in GraphPad® Prism. Fig. 1 shows the inhibitory activity of the [^{127}I]SIB-conjugated VIP116 and the parent peptide VIP116 towards MDM2 as a function of peptide concentration. The inhibitory potency (IC_{50}) of the SIB-conjugated peptide

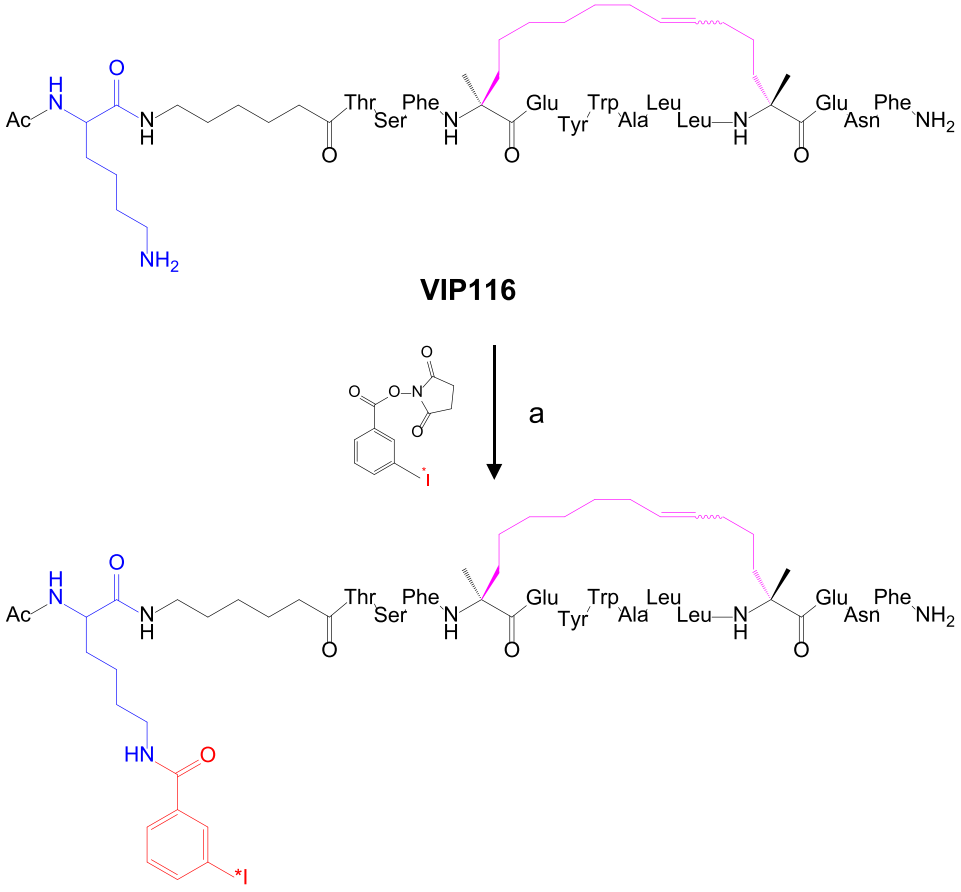

Scheme 1. Radioiodination of the stapled peptide VIP116 with the prosthetic reagent *N*-succinimidyl-3-[*I]iodobenzoate ([*I]SIB). a) DMF, DIEA, RT, 20 min.

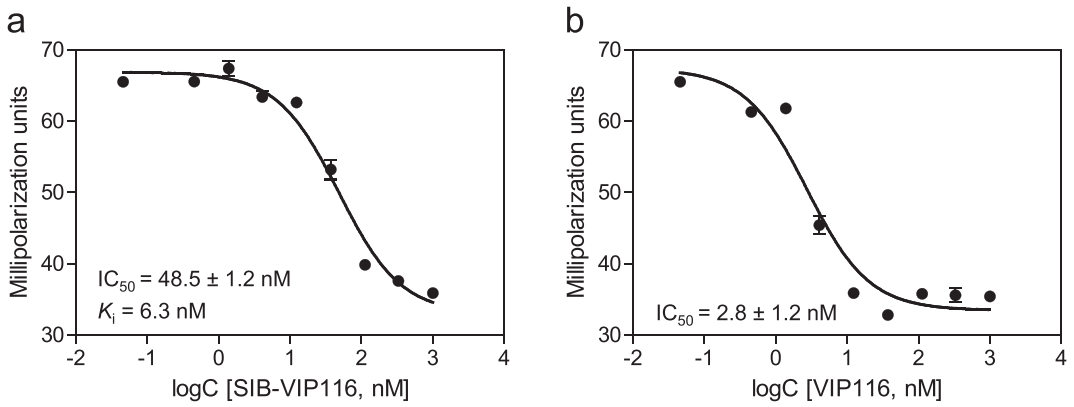

Fig. 1. Determining the inhibitory potency (IC_{50}) of SIB-VIP116 (a) and the parent peptide VIP116 (b) against MDM2 by a fluorescence polarization-based assay. IC_{50} values are shown as mean ± standard error.

[^{127}I]SIB-VIP116 determined from these assays was 48.5 ± 1.2 nM, while unmodified VIP116 had an IC_{50} of 2.8 ± 1.2 nM. The inhibition constant (K_i) of [^{127}I]SIB-VIP116, determined using the IC_{50} value and the binding affinity (K_d: 0.96 nM) parameter of the 5-FAM-PMDM6:MDM2 complex, was 6.3 nM.[28–30] Comparison of the IC_{50} values of the [^{127}I]SIB-VIP116 and the parent peptide VIP116 suggests that SIB conjugation has lowered the peptide's inhibitory activity towards the MDM2:p53 complex. It has been shown previously that stapled peptides containing 1–3 lysine residues on the *N*-terminus of the MDM2 binding template peptide sequence have binding affinities similar to that for a peptide without a lysine residue or the aminohexanoic moiety (e.g., K_d of 19.7 nM for VIP65 vs. 15.1 nM for VIP116).[22] While the lysine and aminohexanoic residues may contribute to improved solubility and cell permeability of the stapled peptide, they do not play a direct role in peptide binding to the critical Phe19-Trp23-Leu26 binding site on the MDM2 protein.[12,22] Nonetheless, the SIB-conjugated stapled peptide displayed a good binding inhibition efficiency (K_i = 6.3 nM) towards MDM2 in the competitive inhibition assays.

Radioiodination of the labeled peptide was achieved similarly to the nonradioactive synthesis but using radioiodinated *N*-succinimidyl-3-[*I] iodobenzoate ([*I]SIB) in two steps.[31] The synthesis of [*I]SIB was accomplished using a tributyltin precursor and *N*-chlorosuccinimide as the oxidizing reagent in 75.9 ± 7.8% yield (n = 8; Fig. S3). Next, conjugation of [*I]SIB to VIP116 (50 μg) was accomplished by incubating the labeling mixture at room temperature for 20 min (Scheme 1), followed by purification using reversed-phase HPLC to obtain the desired [*I]SIB-VIP116 (Fig. S4). The conjugation yield was 46.2 ± 8.0% (n = 7) relative to the starting [^{125}I]SIB activity. The purified [*I]SIB-VIP116 was then subjected to solid-phase extraction (Empore™ C_{18}) to remove acetonitrile and stored in the elution mixture (ethanol:PBS; 60:40) at 4 °C for several days without any significant degradation (97.7% intact at day 7, Fig. S5).

The lipophilicity of [^{125}I]SIB-VIP116 was determined by the shake-flask method using *n*-octanol and phosphate-buffered saline (pH 7.4).[28] A log*D* of 1.45 ± 0.05 (n = 4) was measured, indicating its general lipophilic nature. Using the closely related stapled peptide VIP82, which has a di-lysine extension versus the single lysine residue in VIP116, Thean et al. reported that stapled peptides having *N*-terminus lysine extensions via an aminohexanoic linker can enter cells without inducing significant disruption to the cell membrane.[22] Additionally, in a recent report, Partridge et al. demonstrated a considerable correlation between lipophilicity and cellular permeability of MDM2 binding stapled peptides,[12] implying that lipophilicity may play a critical role in the cellular permeability of radiolabeled stapled peptides as well. We speculate that [*I]SIB conjugation on the lysine residue of VIP116 may have further increased the lipophilicity of the labeled peptide (log*D* = 1.45 ± 0.05) compared to the parent peptide VIP116 and likely contributed to the cellular permeability of the labeled peptide.[32]

Serum stability of the labeled peptide was verified by incubating [^{125}I]SIB-VIP116 with human serum at 37 °C for 72 h. At each time point, an aliquot of serum was analyzed by RP-HPLC connected with a Chromolith® Performance RP-18 column (EMD Millipore) and eluted with gradient mixtures of ethanol and sodium acetate buffer (0.05 M, pH 5.5) at a flow rate of 1 mL per minute.[28] The analyses revealed high serum stability for [^{125}I]SIB-VIP116, with 98.2% of the HPLC-injected activity attributed to the intact labeled peptide at 1 h post-incubation, decreasing only slightly to 96.0% at 72 h post-incubation (Fig. 2).

Studies were conducted to determine the uptake of [^{125}I]SIB-VIP116 in the MDM2-amplified SJSA-1 osteosarcoma cell line (wild-type p53) in a serum-free medium. Cells plated in 24-well plates were incubated with the labeled peptide in RPMI-1640 medium with/without varying concentrations (5–50 μM) of the parent peptide VIP116 for blocking. After a 1 h incubation, cells were washed with PBS three times and lysed with a cell lysis reagent (Promega) to determine the percentage of the added radioactivity retained in the cells. Cell uptake data were normalized to protein concentration for each well and presented as percentage uptake per milligram protein (%/mg protein; Fig. 3). After the 1 h incubation, 12.4 ± 1.4% of the input dose was taken up by SJSA-1 cells, which corresponded to 165.3 ± 27.7%/mg protein (Fig. 3a). Co-incubation of cells with VIP116 (5–50 μM) resulted in a concentration-dependent decrease in the uptake of [^{125}I]SIB-VIP116 by SJSA-1 cells, with the highest blocking effect (~80%) observed at 50 μM VIP116. Next, the kinetics of [^{125}I]SIB-VIP116 uptake in SJSA-1 cells was assessed. For this, the labeled peptide was incubated with the cells for 30–120 min with/without 50 μM VIP116. The uptake of [^{125}I]SIB-VIP116 increased from 104 ± 11%/mg protein at 30 min to 142.4 ± 7.9%/mg protein at 60 min, but no significant increase was observed after that. However, the nonblocked-to-blocked ratios increased with incubation time, from 2.5 at 0.5 h to 4.6 and 7.1 at 1 h and 2 h, respectively, indicating maximal specific binding at 2 h. Collectively, the cell uptake data confirmed the cellular permeability of [^{125}I]SIB-VIP116 and its binding to MDM2 with high specificity, as indicated by > 85% blocking achieved at 50 μM VIP116 after a 2 h incubation (Fig. 3b).

Next, we assessed the intracellular retention of radioactivity in tumor cells by incubating SJSA-1 cells with [^{125}I]SIB-VIP116 for 1 h for baseline uptake and subsequently reincubating the cells with fresh medium for up to 2 h. Fig. 4 shows the percentage of the initially bound radioactivity retained in cells (left y-axis) and the cumulative rate of release into the cell culture medium (right y-axis) as a function of time. For example, at 0.5 h, 83.1 ± 1.0% of the initially bound radioactivity was retained in the cells, with 16.9 ± 1.0% released into the supernatant. However, the radioactivity released into the supernatants was less pronounced at subsequent time points, with 72.8 ± 1.9%, 66.4 ± 2.0%, and 62.0 ± 1.9% of initially bound activity remaining cell-associated at 1.0,

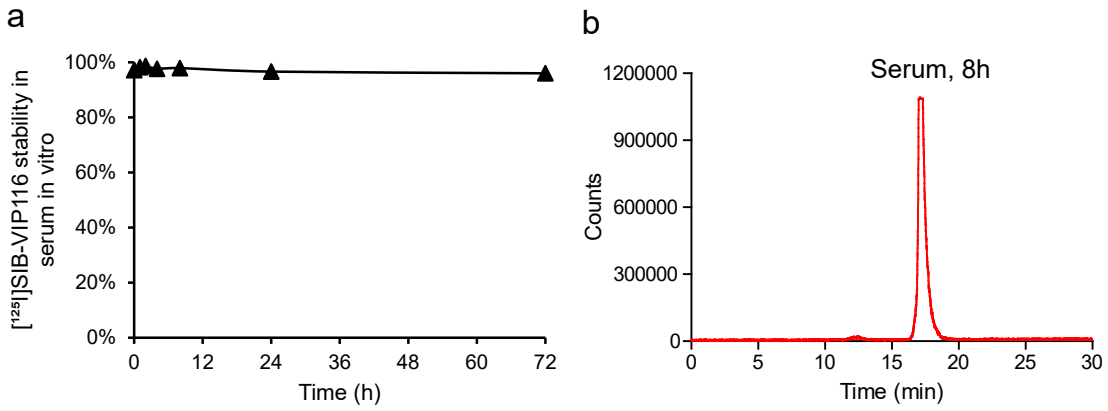

Fig. 2. Serum stability of the [^{125}I]SIB-labeled VIP116 in vitro. (A) Percentage of intact [^{125}I]SIB-VIP116 in human serum after 1–72 h incubation at 37 °C. (B) Representative HPLC chromatogram of the serum sample analyzed at 8 h post-incubation with [^{125}I]SIB-VIP116 (97.9%).

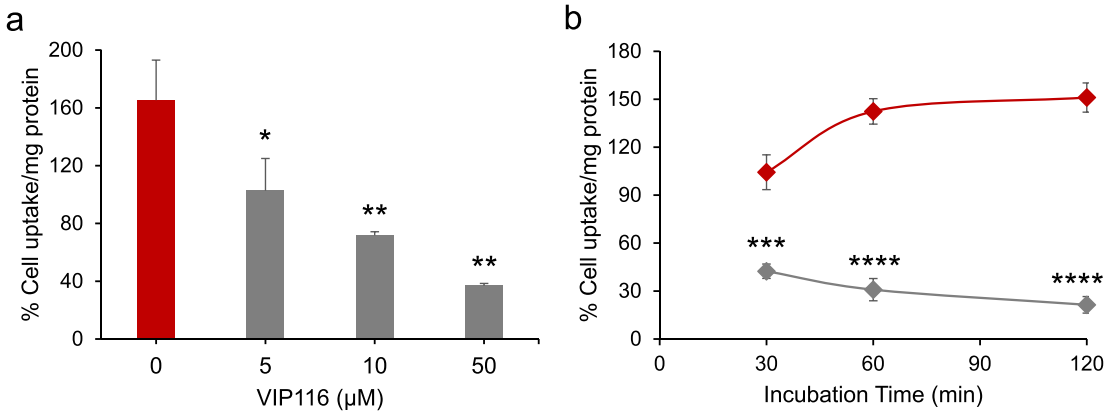

Fig. 3. Uptake of [^{125}I]SIB-VIP116 in MDM2 expressing wild-type p53 SJSA-1 tumor cells. (a) Cells were co-incubated with [^{125}I]SIB-VIP116 and varying concentrations of VIP116 (0–50 μM) to assess [^{125}I]SIB-VIP116 uptake for 1 h. (b) Uptake of [^{125}I]SIB-VIP116 in SJSA-1 cells with (grey) or without (red) VIP116 (50 μM) at different time points post-incubation. Data are shown as mean ± SD for triplicates. *$p \leq 0.05$, **$p \leq 0.01$, ***$p \leq 0.001$, ****$p \leq 0.0001$ vs. no VIP116 co-incubation (0 μM).

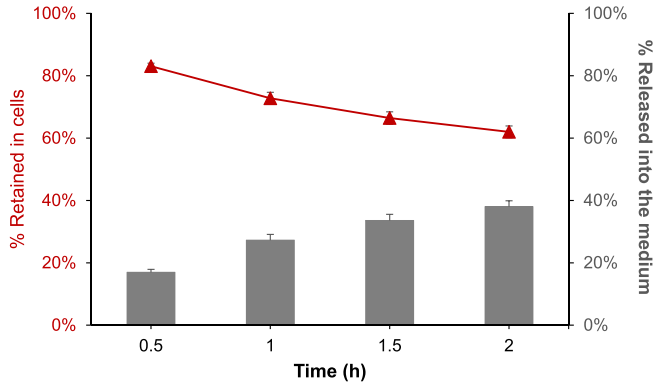

Fig. 4. Uptake and efflux of [^{125}I]SIB-VIP116 in SJSA-1 tumor cells. Cells were incubated with [^{125}I]SIB-VIP116 for 1 h and reincubated with fresh medium for 0.5–2 h. Left and right Y-axes show the percentage of the initially bound activity retained in the cells vs. that released (cumulative %) into the supernatant medium at 0.5–2 h after reincubation.

1.5, and 2.0 h, respectively. These results suggest significant retention and slow washout of the labeled peptide from MDM2-expressing SJSA-1 tumor cells.

The tumor uptake and normal tissue distribution characteristics of [^{125}I]SIB-VIP116 were evaluated in athymic mice bearing SJSA-1 tumor xenografts in the flank region. Groups of five mice (n = 5) were injected with [^{125}I]SIB-VIP116 (166.5 kBq, 100 μL) via the tail vein, and the radioactivity levels in tumors, blood, and major organs were determined at 0.5–24 h after injection by gamma counting (Table 1). Consistent with

Table 1
Whole body biodistribution data for [^{125}I]SIB-VIP116 in mice bearing SJSA-1 human osteosarcoma xenografts.[1]

Organ	30 min	2 h	6 h	24 h
Liver	13.52 ± 6.18	18.41 ± 1.45	11.41 ± 4.46	4.72 ± 2.84
Spleen	1.29 ± 0.61	1.80 ± 0.65	1.99 ± 0.44	0.58 ± 0.24
Lungs	4.27 ± 1.06	2.72 ± 1.16	2.49 ± 1.17	0.33 ± 0.19
Heart	2.52 ± 0.49	2.44 ± 0.49	2.14 ± 0.38	0.37 ± 0.08
Kidneys	3.06 ± 1.82	2.54 ± 0.50	2.50 ± 0.48	0.63 ± 0.12
Bladder	0.61 ± 0.21	0.58 ± 0.34	0.95 ± 0.78	0.29 ± 0.09
Stomach	0.34 ± 0.09	0.53 ± 0.17	1.90 ± 1.15	0.84 ± 0.43
Sm. Int.	0.43 ± 0.09	2.17 ± 0.99	3.84 ± 1.29	0.86 ± 0.35
Lg. Int.	0.06 ± 0.06	0.24 ± 0.20	4.44 ± 1.90	1.87 ± 1.29
Thyroid	0.89 ± 0.17	1.14 ± 0.43	1.19 ± 0.36	0.27 ± 0.14
Muscle	0.16 ± 0.06	0.24 ± 0.07	0.25 ± 0.11	0.16 ± 0.09
Blood	8.33 ± 1.18	6.84 ± 1.92	5.12 ± 0.90	0.62 ± 0.20
Tumor	1.80 ± 0.75	2.19 ± 0.56	2.11 ± 0.29	0.36 ± 0.12
Bone	0.38 ± 0.19	0.33 ± 0.23	0.29 ± 0.20	0.16 ± 0.04
Skin	0.57 ± 0.17	0.88 ± 0.18	1.22 ± 0.47	0.52 ± 0.13
Brain	0.24 ± 0.13	0.25 ± 0.08	0.20 ± 0.06	0.02 ± 0.01
tumor/blood	0.22 ± 0.10	0.32 ± 0.02	0.42 ± 0.08	0.62 ± 0.20
tumor/muscle	11.95 ± 5.68	9.43 ± 1.69	6.82 ± 0.86	3.46 ± 2.57

[1] Data presented as %ID/g (n = 5/time point).

its lipophilic nature, the labeled peptide was cleared primarily via the liver. At 30 min, the radioactivity level in the liver was 13.52 ± 6.18 percent injected dose per gram (% ID/g), which increased to 18.41 ± 1.45% ID/g at 2 h but cleared with time to 4.72 ± 2.84% ID/g at 24 h. The activity concentration in the blood was highest at 30 min, 8.33 ± 1.18% ID/g, which cleared slowly to 5.12 ± 0.90% ID/g at 6 h and 0.62 ± 0.20% ID/g at 24 h. In tumors, the uptake of [^{125}I]SIB-VIP116 increased from 1.80 ± 0.75% ID/g at 30 min to 2.19 ± 0.56% ID/g at 2 h, and remained at similar levels at 6 h (2.11 ± 0.29% ID/g). At 24 h, the radioactivity levels in tumors decreased significantly, to 0.36 ± 0.12% ID/g. Consistent with the stability of the 3-[*I]iodobenzoate ([*I]SIB) template towards dehalogenation in vivo, radioactivity uptake in the thyroid gland remained low (0.27 ± 0.14% ID/g at 24 h). Likely reflecting its lipophilic nature, [^{125}I]SIB-VIP116 exhibited minimal excretion via the kidneys, with ≤0.93% ID found in the urine at 2 h (data not shown). Comparison of the radioactivity levels in tumors with that in muscle revealed maximal tumor-to-muscle ratios of 11.9 ± 5.7 at 30 min. The tumor-to-muscle ratios decreased at subsequent time points to 9.4 ± 1.7 and 6.8 ± 0.9 at 2 h and 6 h, respectively. Conversely, the tumor-to-blood ratios were <1.0 at all time points due to the high levels of radioactivity in the blood.

Metabolic studies were conducted to determine the in vivo stability of the labeled stapled peptide in athymic mice without tumors. Mice were injected with [^{131}I]SIB-VIP116 via the tail vein; plasma and urine samples were collected at 2 h and 4 h post-injection (n = 2/time point) and analyzed by RP-HPLC as described for the in vitro serum stability studies. Fig. 5 shows the HPLC profiles of the plasma samples collected at 2 h and 4 h post-injection. At 2 h, approximately 68% of the radioactivity in plasma was attributable to the intact labeled peptide (t_R = 20.1 min), and the remainder (32%) of the activity was associated with a polar peak eluting at 4.4 min. At 4 h, the intact labeled peptide corresponded to about 80% of the radioactivity in plasma, and the polar peak accounted for the remaining 20%. Consistent with the biodistribution data showing the liver as the primary organ of clearance for [^{125}I]SIB-VIP116, no intact labeled peptide could be detected in the urine at 2 h and 4 h p.i. (Fig. S6). However, the low levels of radioactivity excreted into the urine were present as a hydrophilic species (t_R = 15.0 min) relative to the retention time of the intact labeled peptide (t_R = ~20.0 min). In addition, about 18% of the radioactivity in urine samples at 4 h was attributable to the same hydrophilic peak that was detected in plasma samples (t_R = 4.3 min), which is consistent with urinary excretion of the polar peak observed in the plasma, albeit at a slower rate.

To the best of our knowledge, this is one of the first studies investigating the potential utility of a stapled peptide scaffold for radiolabeled probe development, specifically for MDM2. Importantly, we have investigated the cellular uptake and tissue distribution characteristics of the stapled peptide [*I]SIB-VIP116 delivered intravenously at radiotracer levels in mice. Concerning previous reports on radiolabeling of stapled peptides, the closely related MDM2-binding stapled peptide PM2 was labeled with ^{125}I by direct iodination of the tyrosine residue of the main peptide template using Chloramine-T.[25] The resulting labeled peptide [^{125}I]I-PM2 showed a high uptake (~20% ID/g) and prolonged retention (up to 48 h) in HCT116 tumor xenografts in mice. However, in that study, [^{125}I]I-PM2 was locally administered on the tumor mass, bypassing the systemic circulation.[25] Additionally, as can be expected for a direct radioiodination on a tyrosine residue, the uptake in the thyroid gland increased with time, suggesting that significant dehalogenation of [^{125}I]I-PM2 had occurred. In contrast, the [*I]SIB labeling method employed for VIP116 in the present study provided a highly stable peptide conjugate towards dehalogenation with only a minimal increase in the thyroid uptake of the radioactivity at 2 h and 6 h compared to that at 30 min. More recently, Hu et al. reported in an abstract the labeling of a different MDM2-binding stapled peptide, STP, with ^{64}Cu via a DOTA chelator at the *N*-terminus of the peptide.[33] The biodistribution characteristics of the resulting [^{64}Cu]Cu-DOTA-STP stapled peptide were investigated in C57BL/6J mice bearing MC38 murine colon carcinoma xenografts after i.v. injection. Potential differences in the peptide sequence, tumor models, and the radionuclide must be considered when comparing the tumor uptake of [^{64}Cu]Cu-DOTA-STP and [*I]SIB-VIP116. Nonetheless, [^{64}Cu]Cu-DOTA-STP showed a maximal tumor uptake of 9.4 ± 1.9% ID/g in MC38 xenografts at 3 h p.i., which is considerably higher than that displayed by [^{125}I]SIB-VIP116 (2.19 ± 0.56 %ID/g) in the SJSA-1 tumor model. In addition to its clearance via the liver, [^{64}Cu]Cu-DOTA-STP also exhibited high levels of radioactivity in the blood at early time points (e.g., ~30% ID/g at 1 h).[33] This likely contributed to its higher tumor uptake than that observed for [*I]SIB-VIP116 in this study, but in general both the labeled peptides displayed less favorable tumor-to-blood ratios, especially at early time points post-injection.[33]

Recently, several approaches have been reported to extend the plasma half-life of radiolabeled peptides by attaching an albumin-binding moiety, Evans blue. In general, there is a concomitant increase in the tumor uptake and tumor-to-background ratios for the labeled peptides compared to those without an albumin-binding moiety.[34,35] In that regard, the slow blood clearance (up to 6 h) and high in vivo stability of [*I]SIB-VIP116 are significant advantages. Nevertheless, it would be beneficial to increase the tumor uptake of [*I]SIB-VIP116 further to improve the tumor-to-blood and tumor-to-normal organ ratios, ideally within 6 h after injection. More recently, peptides sequences based on all D-amino acids have been explored for developing MDM2-binding stapled peptides with high proteolytic stability and cellular activity.[12,36] From these studies, ^{d}PMI-δ(1-5-12), consisting of two staples with a common attachment point at residue 5 of the peptide template has emerged as a lead peptide with a high binding affinity towards MDM2 (and the homologous MDM4), and improved α-helicity (52%) and high proteolytic stability.[36] Thus, future studies should include radiolabeling and evaluating D-amino acid-based peptides, such as ^{d}PMI-δ(1-5-12), using [*I]SIB or conceptually similar prosthetic

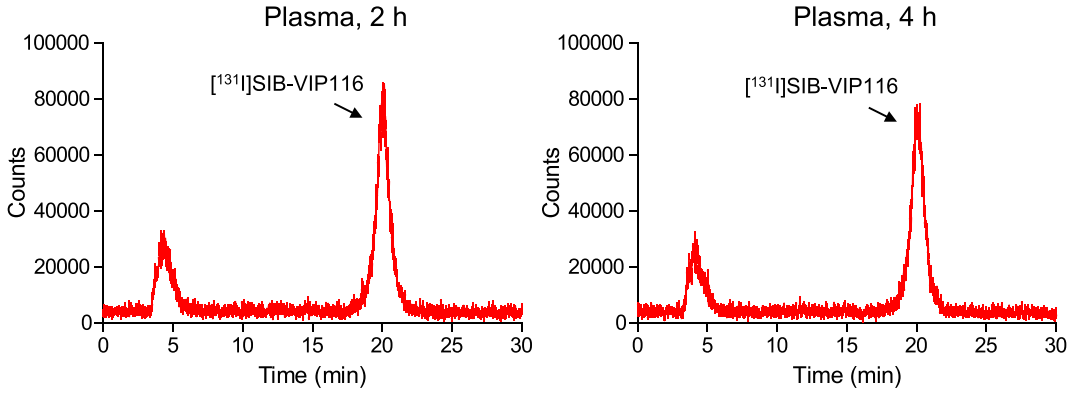

Fig. 5. In vivo stability analysis of ^{131}I-labeled VIP116, [^{131}I]SIB-VIP116, in athymic mice at 2 h and 4 h after intravenous injection.

agents.

In summary, we have successfully radiolabeled a MDM2 binding stapled peptide, VIP116, with radioiodine using *N*-succinimidyl-3-[*I] iodobenzoate ([*I]SIB) under mild reaction conditions. The radioiodinated stapled peptide demonstrated efficient cell uptake, specificity, and good retention of the radioactivity in SJSA-1 tumor cells. Furthermore, in vivo studies confirmed the metabolic stability of [*I]SIB-VIP116 and indicated a moderate uptake in SJSA-1 xenografts in mice after intravenous administration. Our results suggest that stapled peptides are promising scaffolds for radiotracer development for intracellular targets such as MDM2 and warrant further evaluation of the ^{124}I/^{123}I-labeled VIP116 and related stapled peptide versions by PET/SPECT imaging.

Declaration of Competing Interest

The authors declare that they have no known competing financial interests or personal relationships that could have appeared to influence the work reported in this paper.

Acknowledgments

The authors thank Xiao-Guang Zhao for outstanding technical support with the biodistribution studies. In addition, the authors gratefully acknowledge Dr. Fernando Ferrer at the Agency for Science Technology and Research (A*STAR), Singapore, for the VIP116 stapled peptide. This research was supported by Grant CA241823 from the National Cancer Institute.

Appendix A. Supplementary data

Supplementary data to this article can be found online at https://doi.org/10.1016/j.bmcl.2022.128725.

References

1 Hennrich U, Benešová M. [^{68}Ga]Ga-DOTA-TOC: The first FDA-approved ^{68}Ga-radiopharmaceutical for PET imaging. *Pharmaceuticals (Basel)*. 2020;13:38. https://doi.org/10.3390/ph13030038.
2 Hennrich U, Kopka K, Lutathera®. The first FDA- and EMA-approved radiopharmaceutical for peptide receptor radionuclide therapy. *Pharmaceuticals*. 2019;12(3). https://doi.org/10.3390/ph12030114.
3 Kimura Richard H, Wang Ling, Shen Bin, et al. Evaluation of integrin $\alpha v\beta_6$ cystine knot PET tracers to detect cancer and idiopathic pulmonary fibrosis. *Nat Commun*. 2019;10. https://doi.org/10.1038/s41467-019-11863-w.
4 Baratto L, Jadvar H, Iagaru A. Prostate cancer theranostics targeting gastrin-releasing peptide receptors. *Mol Imaging Biol*. 2018;20(4):501–509. https://doi.org/10.1007/s11307-017-1151-1.
5 Zhou X, Jiang J, Yang X, et al. First-in-human evaluation of a PD-L1-binding peptide radiotracer in non-small cell lung cancer patients with PET. *J Nucl Med*. 2021. https://doi.org/10.2967/jnumed.121.262045.
6 Vinogradov AA, Yin Y, Suga H. Macrocyclic peptides as drug candidates: recent progress and remaining challenges. *J Am Chem Soc*. 2019;141:4167–4181. https://doi.org/10.1021/jacs.8b1317810.1021/jacs.8b13178.s001.
7 Vag T, Gerngross C, Herhaus P, et al. First experience with chemokine receptor CXCR4-targeted PET imaging of patients with solid cancers. *J Nucl Med*. 2016;57:741–746. https://doi.org/10.2967/jnumed.115.161034.
8 Hofman MS, Lau WF, Hicks RJ. Somatostatin receptor imaging with ^{68}Ga DOTATATE PET/CT: clinical utility, normal patterns, pearls, and pitfalls in interpretation. *Radiographics*. 2015;35:500–516. https://doi.org/10.1148/rg.352140164.
9 Walensky LD, Bird GH. Hydrocarbon-stapled peptides: principles, practice, and progress. *J Med Chem*. 2014;57:6275–6288. https://doi.org/10.1021/jm4011675.
10 Bernal F, Tyler Andrew F, Korsmeyer Stanley J, Walensky Loren D, Verdine Gregory L. Reactivation of the p53 tumor suppressor pathway by a stapled p53 peptide. *J Am Chem Soc*. 2007;129:2456–2457. https://doi.org/10.1021/ja069358710.1021/ja0693587.s001.
11 Chang YS, Graves B, Guerlavais V, et al. Stapled alpha-helical peptide drug development: a potent dual inhibitor of MDM2 and MDMX for p53-dependent cancer therapy. *Proc Natl Acad Sci U S A*. 2013;110:E3445–3454. https://doi.org/10.1073/pnas.1303002110.
12 Partridge Anthony W, Kaan Hung Yi Kristal, Juang Yu-Chi, et al. Incorporation of putative helix-breaking amino acids in the design of novel stapled peptides: exploring biophysical and cellular permeability properties. *Molecules*. 2019;24:2292. https://doi.org/10.3390/molecules24122292.
13 Saleh MN, Patel MR, Bauer TM, et al. Phase 1 trial of ALRN-6924, a dual inhibitor of MDMX and MDM2, in patients with solid tumors and lymphomas bearing wild-type TP53. *Clin Cancer Res*. 2021. https://doi.org/10.1158/1078-0432.CCR-21-0715.
14 Brown Christopher J, Quah Soo T, Jong Janice, et al. Stapled peptides with improved potency and specificity that activate p53. *ACS Chem Biol*. 2013;8:506–512. https://doi.org/10.1021/cb3005148.
15 Kastenhuber ER, Lowe SW. Putting p53 in context. *Cell*. 2017;170:1062–1078. https://doi.org/10.1016/j.cell.2017.08.028.
16 Piette J, Neel H, Marechal V. Mdm2: Keeping p53 under control. *Oncogene*. 1997;15(9): 1001-1010. https://doi.org/DOI 10.1038/sj.onc.1201432.
17 Shieh SY, Ikeda M, Taya Y, Prives C. DNA damage-induced phosphorylation of p53 alleviates inhibition by MDM2. *Cell*. 1997;91:325–334. https://doi.org/10.1016/s0092-8674(00)80416-x.
18 Oliner JD, Kinzler KW, Meltzer PS, George DL, Vogelstein B. Amplification of a gene encoding a P53-associated protein in human sarcomas. *Nature*. 1992;358: 80-83. https://doi.org/DOI 10.1038/358080a0.
19 Forslund Ann, Zeng Zhaoshi, Qin Li-Xuan, et al. MDM2 gene amplification is correlated to tumor progression but not to the presence of SNP309 or TP53 mutational status in primary colorectal cancers. *Mol Cancer Res*. 2008;6:205–211. https://doi.org/10.1158/1541-7786.MCR-07-0239.
20 Gluck W Larry, Gounder Mrinal M, Frank Richard, et al. Phase 1 study of the MDM2 inhibitor AMG 232 in patients with advanced P53 wild-type solid tumors or multiple myeloma. *Invest New Drugs*. 2020;38:831–843. https://doi.org/10.1007/s10637-019-00840-1.
21 Andreeff Michael, Kelly Kevin R, Yee Karen, et al. Results of the phase I trial of RG7112, a small-molecule MDM2 antagonist in leukemia. *Clin Cancer Res*. 2016;22:868–876.
22 Thean D, Ebo JS, Luxton T, et al. Enhancing specific disruption of intracellular protein complexes by hydrocarbon stapled peptides using lipid based delivery. *Sci Rep*. 2017;7. https://doi.org/10.1038/s41598-017-01712-5.
23 Yuen Tsz Ying, Brown Christopher J, Xue Yuezhen, et al. Stereoisomerism of stapled peptide inhibitors of the p53-Mdm2 interaction: an assessment of synthetic strategies and activity profiles. *Chem Sci*. 2019;10:6457–6466. https://doi.org/10.1039/C9SC01456J.
24 Lundsten Sara, Hernández Víctor Agmo, Gedda Lars, et al. Tumor-Targeted Delivery of the p53-Activating Peptide VIP116 with PEG-Stabilized Lipodisks. *Nanomaterials (Basel)*. 2020;10:783. https://doi.org/10.3390/nano10040783.
25 Spiegelberg D, Mortensen AC, Lundsten S, Brown CJ, Lane DP, Nestor M. The MDM2/MDMX-p53 antagonist PM2 radiosensitizes wild-type p53 tumors. *Cancer Res*. 2018;78:5084–5093. https://doi.org/10.1158/0008-5472.CAN-18-0440.
26 Mortensen ACL, Morin E, Brown CJ, Lane DP, Nestor M. Enhancing the therapeutic effects of in vitro targeted radionuclide therapy of 3D multicellular tumor spheroids using the novel stapled MDM2/X-p53 antagonist PM2. *EJNMMI Res*. 2020;10:38. https://doi.org/10.1186/s13550-020-0613-7.
27 Chen H, Niu G, Wu H, Chen X. Clinical application of radiolabeled RGD peptides for PET imaging of integrin $\alpha v\beta_3$. *Theranostics*. 2016;6:78–92. https://doi.org/10.7150/thno.13242.
28 Zhou Zhengyuan, Zalutsky Michael R, Chitneni Satish K. Fluorine-18 labeling of the MDM2 inhibitor RG7388 for PET imaging: chemistry and preliminary evaluation. *Mol Pharm*. 2021;18:3871–3881. https://doi.org/10.1021/acs.molpharmaceut.1c00531.
29 Nikolovska-Coleska Zaneta, Wang Renxiao, Fang Xueliang, et al. Development and optimization of a binding assay for the XIAP BIR3 domain using fluorescence polarization. *Anal Biochem*. 2004;332:261–273. https://doi.org/10.1016/j.ab.2004.05.055.
30 Ding Ke, Lu Yipin, Nikolovska-Coleska Zaneta, et al. Structure-based design of potent non-peptide MDM2 inhibitors. *J Am Chem Soc*. 2005;127:10130–10131. https://doi.org/10.1021/ja051147z10.1021/ja051147z.s001.
31 Chitneni Satish K, Koumarianou Eftychia, Vaidyanathan Ganesan, Zalutsky Michael R. Observations on the effects of residualization and dehalogenation on the utility of *N*-succinimidyl ester acylation agents for radioiodination of the internalizing antibody trastuzumab. *Molecules*. 2019;24:3907. https://doi.org/10.3390/molecules24213907.
32 Waring MJ. Lipophilicity in drug discovery. *Expert Opin Drug Discov*. 2010;5:235–248. https://doi.org/10.1517/17460441003605098.
33 Hu K, Xie L, Zhang Y, Hanyu M, Zhang M-R. Stapled Peptide-based radiotheranostics agent targeting MDM2 suppresses p53-mutant tumor growth. *J Nucl Med*. 2021;62(supplement 1):3.
34 Tian Rui, Jacobson Orit, Niu Gang, et al. Evans Blue attachment enhances somatostatin receptor subtype-2 imaging and radiotherapy. *Theranostics*. 2018;8:735–745. https://doi.org/10.7150/thno.23491.
35 Li Y, Li D, Wu H, Huang J, Cheng Z. Synthesis and application of a long-circulating radiolabeled peptide for targeting of osteosarcoma. *Mol Imaging Biol*. 2020;22:940–947. https://doi.org/10.1007/s11307-019-01468-6.
36 Kannan S, Aronica PGA, Ng S, et al. Macrocyclization of an all-d linear alpha-helical peptide imparts cellular permeability. *Chem Sci*. 2020;11:5577–5591. https://doi.org/10.1039/c9sc06383h.